

Distributional Ergodicity in Stored-Energy-Driven Lévy Flights

Takuma Akimoto^{1,*} and Tomoshige Miyaguchi^{2,†}

¹*Department of Mechanical Engineering, Keio University, Yokohama, 223-8522, Japan*

²*Department of Mathematics Education, Naruto University of Education, Tokushima 772-8502, Japan*

(Dated: September 14, 2018)

We study a class of random walk, the stored-energy-driven Lévy flight (SEDLF), whose jump length is determined by a stored energy during a trapped state. The SEDLF is a continuous-time random walk with jump lengths being coupled with the trapping times. It is analytically shown that the ensemble-averaged mean square displacements exhibit subdiffusion as well as superdiffusion, depending on the coupling parameter. We find that time-averaged mean square displacements increase linearly with time and the diffusion coefficients are intrinsically random, a manifestation of *distributional ergodicity*. The diffusion coefficient shows aging in subdiffusive regime, whereas it increases with the measurement time in superdiffusive regime.

I. INTRODUCTION

Single particle tracking experiments in biological systems often show that diffusion is not normal but rather anomalous [1–6]; that is, the mean square displacement (MSD) does not grow linearly with time but follows a power-law scaling

$$\langle x_t^2 \rangle \propto t^\beta \quad (\beta \neq 1). \quad (1)$$

Because anomalous diffusions including subdiffusion ($\beta < 1$) as well as superdiffusion ($\beta > 1$) are ubiquitously observed in many biological experiments, anomalous diffusion is believed to play significant roles in cell biology such as gene regulation [7] and active transports [1, 6]. However, the underlying physical mechanisms remain controversial.

To understand the underlying mechanisms of these anomalous diffusions, phenomenological models such as continuous-time random walk (CTRW), Lévy walk and flight, and other stochastic models of anomalous diffusion have been intensively studied [5, 8–13]. Among these models, CTRW shows a prominent feature called *distributional ergodicity* [10–12, 14]; that is, the time average of an observable converges to a random variable, i.e., *convergence in distribution*, but it does not coincide with the ensemble average as in the ordinary sense of ergodicity. It is considered that this distributional behavior of time-averaged observables in CTRW is related to large fluctuations of transport coefficients in single particle tracking experiments [2–5]. It is known that such distributional behavior is universal in *infinite ergodic theory* [15, 16], where ergodicity is satisfied with respect to an infinite (non-normalizable) invariant measure. This is a completely different feature from other stochastic models of subdiffusion.

While uncoupled CTRWs, in which trapping time and jump length are mutually independent, are extensively

studied, effects of a coupling between them become physically important for nonthermal systems such as cells [1, 6]. In such nonthermal systems, a particle in a trapped state would not be simply frozen, but rather it would be storing a sort of energy for the next jump. Thus, a random walk driven by an stored energy during a trapped state is essential in such nonthermal systems, and it will also be important in complex systems such

as finance [17] and earthquakes [18].

As a prototype model of such nonthermal random walks, we study a CTRW with jump lengths correlated with trapping times [19–21], which we refer to as the stored-energy-driven Lévy flight (SEDLF). The SEDLF exhibits a whole spectrum of diffusion: sub-, normal-, and super-diffusion, depending on a parameter γ , which characterizes the coupling strength between jump length and trapping time. Here, we show a novel type of distributional ergodicity. In particular, time-averaged observables such as the time-averaged MSDs (TAMSDs) are intrinsically random even when the measurement time goes to infinity.

II. MODEL

The SEDLF is based on CTRW with a non-separable joint probability of trapping time and jump length. In general, CTRW is defined through the joint probability density function (PDF) $\psi(x, t)$, where $\psi(x, t)dxdt$ is the probability that a random walker jumps with length $[x, x+dx]$ just after it is trapped for period $[t, t+dt]$ since its previous jump [22, 23]. In particular, the separable case $\psi(x, t) = w(t)l(x)$, in which the jump length and the trapping time are mutually independent, has been extensively studied [8, 10–12, 24]. Here, we consider a non-separable case defined by

$$\psi(x, t) = w(t) \frac{\delta(x - t^\gamma) + \delta(x + t^\gamma)}{2}, \quad (2)$$

where $w(t)$ is the PDF of trapping times and $\gamma \in [0, 1]$ is a coupling strength. Note that a random walker undergoes a long trapped state before it performs a long

* akimoto@z8.keio.jp

† tmiyaguchi@naruto-u.ac.jp

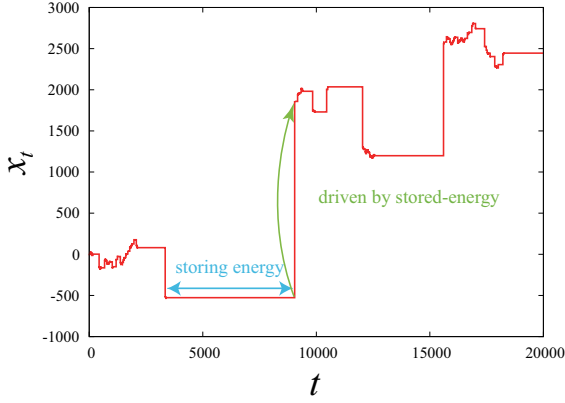


FIG. 1. A trajectory of SEDLF ($\alpha = 0.7$ and $\gamma = 0.9$). A big jump occurs when a random walker is trapped for a long time.

jump (Fig. 1). In addition, we assume that the PDF of trapping times follows a power law:

$$w(t) \simeq \frac{c_0}{t^{1+\alpha}}, \quad (3)$$

as $t \rightarrow \infty$. Here, $\alpha \in (0, 1)$ is the stable index, a constant c_0 is defined by $c_0 = c/|\Gamma(-\alpha)|$ with a scale factor c .

For $\gamma = 0$, the SEDLF is just a separable CTRW with jumps only to the nearest neighbor sites. On the other hand, for $\gamma > 0$, the PDF of jump follows a power law:

$$l(x) = \int_0^\infty \psi(x, t) dt = \frac{|x|^{\frac{1}{\gamma}-1}}{2\gamma} w\left(|x|^{\frac{1}{\gamma}}\right) \simeq \frac{c_0}{2\gamma} \frac{1}{|x|^{1+\alpha/\gamma}}. \quad (4)$$

Thus, the mean jump length diverges for $\gamma \geq \alpha$. Note that the Lévy flight also has a power law distribution of jump length, which causes a divergence in the MSD. By contrast, the MSD of the SEDLF is finite with the aid of the coupling between jump lengths and trapping times as shown below. This property makes the SEDLF a physically more coherent model than Lévy flight.

III. THEORY

Generalized master equations for CTRWs obtained in [22] can be utilized for our model. In general, the spacial distribution $P(x, t)$ of CTRWs with initial distribution $P_0(x)$ at time zero satisfies the following equations:

$$P(x, t) = \int_0^t dt' \Psi(t-t') Q(x, t') + \Psi_0(t) P_0(x), \quad (5)$$

$$Q(x, t) = \int_{-\infty}^\infty dx' \int_0^t dt' \psi(x', t') Q(x-x', t-t') + \int_{-\infty}^\infty dx' \psi_0(x', t) P_0(x-x'), \quad (6)$$

where $Q(x, t) dt dx$ is the probability of a random walker reaching an interval $[x, x+dx]$ just in a period $[t, t+dt)$,

$\Psi(t)$ is the probability of being trapped for longer than time t :

$$\Psi(t) = 1 - \int_{-\infty}^\infty dx' \int_0^t \psi(x', t') dt' = 1 - \int_0^t w(t') dt', \quad (7)$$

$\psi_0(x, t)$ is the joint PDF for the first jump, and $\Psi_0(t)$ is the probability that the first jump does not occur until time t . Fourier-Laplace transform with respect to space and time ($x \rightarrow k$ and $t \rightarrow s$, respectively), defined by

$$\hat{P}(k, s) \equiv \int_{-\infty}^\infty dx \int_0^\infty dt P(x, t) e^{ikx} e^{-st}, \quad (8)$$

gives

$$\hat{P}(k, s) = \frac{\hat{P}_0(k)}{1 - \hat{\psi}(k, s)} \frac{1 - \hat{w}_0(s) + \hat{\varphi}_0(k, s)}{s}, \quad (9)$$

where $\hat{\varphi}_0(k, s) = [1 - \hat{w}(s)] \hat{\psi}_0(k, s) - [1 - \hat{w}_0(s)] \hat{\psi}(k, s)$.

In the case of the SEDLF, we obtain $\hat{\psi}(k, s)$ from Eq. (2) as follows

$$\hat{\psi}(k, s) = \int_0^\infty e^{-st} \cos(kt^\gamma) w(t) dt. \quad (10)$$

Note that $\hat{\psi}(0, s) = \hat{w}(s)$, and the asymptotic behavior of the Laplace transform of $w(t)$ [Eq. (3)] is given by

$$1 - \hat{w}(s) \simeq cs^\alpha \quad (s \rightarrow 0). \quad (11)$$

We assume that the initial distribution $P_0(x)$ is the delta function, $P_0(x) = \delta(x)$, and $w(t) = w_0(t)$ (ordinary renewal process [25]). As a result, we have the following generalized master equation in the Fourier and Laplace space:

$$\hat{P}(k, s) = \frac{1}{s} \frac{1 - \hat{w}(s)}{1 - \hat{\psi}(k, s)}, \quad (12)$$

where $\hat{\psi}(k, s)$ and $\hat{w}(s)$ are given by Eqs. (10) and (11).

Here, we derive the asymptotic behavior of the moments of position x_t for $t \rightarrow \infty$ using the Fourier-Laplace transform $\hat{P}(k, s)$. The Laplace transform of $\langle x_t \rangle$, denoted by $\langle x_s \rangle$, is given by

$$\langle x_s \rangle = -i \frac{\partial \hat{P}(k, s)}{\partial k} \Big|_{k=0} = 0, \quad (13)$$

which means there is no drift, $\langle x_t \rangle = 0$. Similarly, the Laplace transform of the second moment, i.e., the ensemble-averaged MSD (EAMSD), is given by

$$\langle x_s^2 \rangle = -\frac{\partial^2 \hat{P}(k, s)}{\partial k^2} \Big|_{k=0} = -\frac{1}{s} \frac{\hat{\psi}''(0, s)}{1 - \hat{w}(s)}. \quad (14)$$

Using the asymptotic behavior at $s \rightarrow 0$, we have

$$\langle x_s^2 \rangle \simeq \begin{cases} \frac{\Gamma(2\gamma - \alpha)}{|\Gamma(-\alpha)|} \frac{1}{s^{1+2\gamma}}, & (2\gamma > \alpha) \\ \frac{1}{|\Gamma(-\alpha)| s^{\alpha+1}} \log\left(\frac{1}{s}\right), & (2\gamma = \alpha) \\ \frac{\langle t^{2\gamma} \rangle}{cs^{\alpha+1}}. & (2\gamma < \alpha) \end{cases} \quad (15)$$

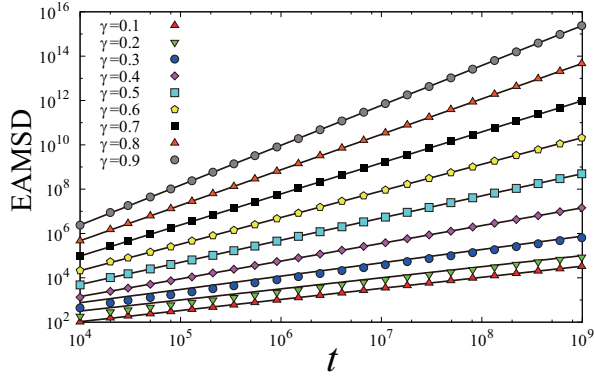


FIG. 2. Ensemble-averaged mean square displacements ($\alpha = 0.5$). Symbols are the results of numerical simulations for different γ with theoretical lines. There are no fitting parameters in the theoretical lines. We set the PDF of the trapping time as $w(t) = \alpha t^{-1-\alpha}$ ($t \geq 1$) in all the numerical simulations. Thus, the jump length PDF is given by $l(x) = \alpha/2\gamma|x|^{1+\alpha/\gamma}$ from Eq. (4), and $\langle l^2 \rangle = \alpha/(\alpha - 2\gamma)$ for $2\gamma < \alpha$.

The inverse Laplace transform for $t \rightarrow \infty$ reads

$$\langle x_t^2 \rangle \simeq \begin{cases} \frac{\Gamma(2\gamma - \alpha)}{|\Gamma(-\alpha)|\Gamma(1 + 2\gamma)} t^{2\gamma}, & (2\gamma > \alpha) \\ \frac{1}{|\Gamma(-\alpha)|\Gamma(1 + \alpha)} t^\alpha \log t, & (2\gamma = \alpha) \\ \frac{\langle l^2 \rangle}{c\Gamma(1 + \alpha)} t^\alpha, & (2\gamma < \alpha) \end{cases} \quad (16)$$

where we used $\langle t^{2\gamma} \rangle = \langle l^2 \rangle = \int_{-\infty}^{\infty} x^2 l(x) dx$. Figure 2 shows the EAMSD for $\alpha = 0.5$. Theory (16) is in excellent agreement with numerical simulations.

It is also possible to derive higher order moments in the following way. By Eq. (12), we have the relation, $\hat{P}(k, s) = \hat{P}(k, s)\hat{\psi}(k, s) + C$, where C does not depend on k . Differentiating both sides n times with respect to k , we have

$$\hat{P}^{(n)}(k, s) = \frac{1}{1 - \hat{\psi}(k, s)} \sum_{l=0}^{n-1} {}_n C_l \hat{P}^{(l)}(k, s) \hat{\psi}^{(n-l)}(k, s). \quad (17)$$

From Eq. (10), we have $\hat{\psi}^{(2n+1)}(0, s) = 0$. Accordingly, we obtain $\hat{P}^{(2n+1)}(0, s) = 0$ and

$$\hat{P}^{(2n)}(0, s) = \frac{1}{1 - \hat{w}(s)} \sum_{l=0}^{n-1} {}_{2n} C_{2l} \hat{P}^{(2l)}(0, s) \hat{\psi}^{(2n-2l)}(0, s), \quad (18)$$

by induction. Thus, $\langle x_t^{2n+1} \rangle = 0$ and the leading order for the Laplace transform of $\langle x_t^{2n} \rangle$ is given by

$$\langle x_s^{2n} \rangle \simeq \begin{cases} \frac{M_n(\alpha, \gamma)}{s^{1+2n\gamma}}, & (2\gamma > \alpha) \\ \frac{(2n)! \{-\hat{\psi}''(0, s)\}^n}{2^n s [1 - \hat{w}(s)]^n}, & (2\gamma \leq \alpha) \end{cases} \quad (19)$$

where $M_n(\alpha, \gamma)$ is given by a recursion relation $M_n(\alpha, \gamma) = \sum_{l=1}^n {}_{2n} C_{2l} M_{n-l}(\alpha, \gamma) \Gamma(2l\gamma - \alpha) / |\Gamma(-\alpha)|$. The above equations (19) can be confirmed by Eq. (18) and mathematical induction. Therefore, the asymptotic behavior for $s \rightarrow 0$ is given by

$$\langle x_s^{2n} \rangle \simeq \begin{cases} \frac{M_n(\alpha, \gamma)}{s^{1+2n\gamma}}, & (2\gamma > \alpha) \\ \frac{(2n)! \{\log(\frac{1}{s})\}^n}{2^n |\Gamma(-\alpha)|^n s^{n\alpha+1}}, & (2\gamma = \alpha) \\ \frac{(2n)! \langle t^{2\gamma} \rangle^n}{(2c)^n s^{n\alpha+1}}, & (2\gamma < \alpha) \end{cases} \quad (20)$$

and the inverse Laplace transform for $t \rightarrow \infty$ reads

$$\langle x_t^{2n} \rangle \simeq \begin{cases} \frac{M_n(\alpha, \gamma)}{\Gamma(1 + 2n\gamma)} t^{2n\gamma}, & (2\gamma > \alpha) \\ \frac{(2n)!}{2^n |\Gamma(-\alpha)|^n \Gamma(1 + n\alpha)} t^{n\alpha} \{\log t\}^n, & (2\gamma = \alpha) \\ \frac{(2n)! \langle l^2 \rangle^n}{(2c)^n \Gamma(1 + n\alpha)} t^{n\alpha}. & (2\gamma < \alpha) \end{cases} \quad (21)$$

It follows that the distribution of a scaled position $x_t / \sqrt{\langle x_t^2 \rangle}$ converges to a time-independent non-trivial distribution. In other words, $x_t / \sqrt{\langle x_t^2 \rangle}$ converges in distribution to $X_{\alpha, \gamma}$ as $t \rightarrow \infty$, where

$$\langle e^{ikX_{\alpha, \gamma}} \rangle = \begin{cases} \sum_{n=0}^{\infty} \frac{(ik)^{2n} M_n(\alpha, \gamma) \Gamma(1 + 2\gamma)^n}{(2n)! M_1(\alpha, \gamma)^n \Gamma(1 + 2n\gamma)}, & (2\gamma > \alpha) \\ \sum_{n=0}^{\infty} \frac{(ik)^{2n} \Gamma(1 + \alpha)^n}{2^n \Gamma(1 + n\alpha)}. & (2\gamma \leq \alpha) \end{cases} \quad (22)$$

We note that the distribution of the random variable $X_{\alpha, \gamma}$ for $2\gamma \leq \alpha$ is called a symmetric Mittag-Leffler distribution of order $\alpha/2$ [26, 27]. Figure 3 shows the PDFs of $X_{\alpha, \gamma}$ for $\gamma = 0.1, 0.6$, and 0.8 ($\alpha = 0.25, 0.5$, and 0.75). For $2\gamma < \alpha$, the PDFs converge to the symmetric Mittag-Leffler distribution, which does not depend on γ . However, the PDFs are different from the symmetric Mittag-Leffler distribution and depend crucially on γ when $2\gamma > \alpha$.

IV. DISTRIBUTIONAL ERGODICITY OF TIME-AVERAGED MEAN SQUARE DISPLACEMENT

Here, we investigate ergodic properties of time-averaged MSD (TAMSD), defined by

$$\overline{\delta^2(\Delta; t)} \equiv \frac{1}{t - \Delta} \int_0^{t-\Delta} [x(t' + \Delta) - x(t')]^2 dt'. \quad (23)$$

It has been known that TAMSD can be represented using the total number of jumps [12, 27], i.e., N_t , and $h_k =$

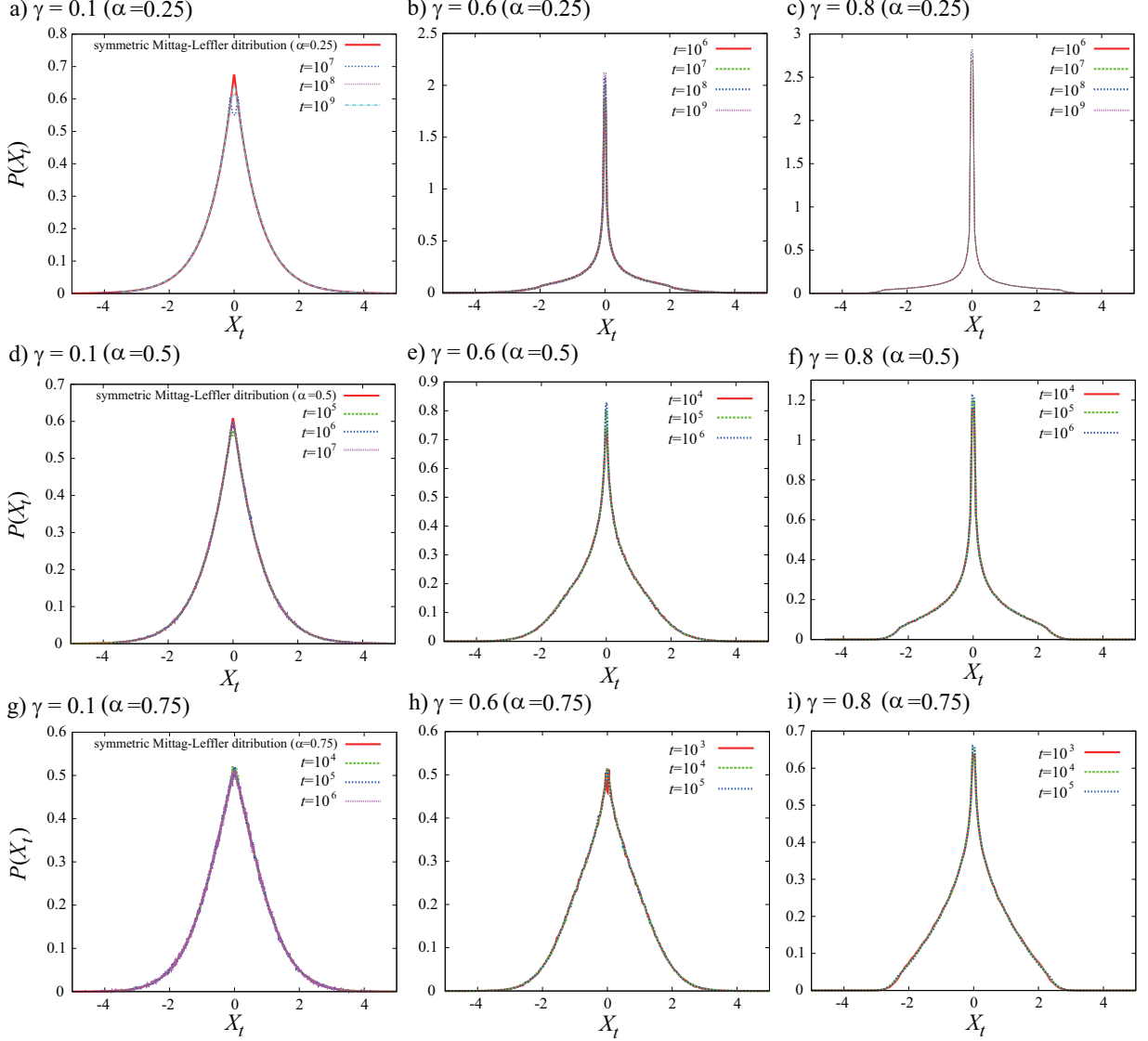


FIG. 3. Probability density functions of a scaled position $X_t = x_t / \sqrt{\langle x_t^2 \rangle}$ ($\alpha = 0.25, 0.5$ and 0.75). PDF $P(X_t)$ converges to a non-trivial PDF as $t \rightarrow \infty$. (a), (d), and (g) the PDFs $P(X_t)$ converge to symmetric Mittag-Leffler distributions ($\gamma = 0.1$). For $2\gamma > \alpha$, the PDFs $P(X_t)$ converge to different distributions depending on α as well as γ . The PDF $w(t)$ used in the numerical simulation is the same as that in Fig. 2.

$$\Delta l_k^2 + 2 \sum_{m=1}^{k-1} l_k l_m \theta(\Delta - t_k + t_m):$$

$$\overline{\delta^2(\Delta; t)} \simeq \frac{1}{t} \sum_{k=0}^{N_t} h_k \quad (t \rightarrow \infty), \quad (24)$$

where l_k is the k th jump, t_k is the time k th jump occurs, and $\theta(t)$ is a step function, defined by $\theta(t) = 0$ for $t < 0$ and t otherwise. One can show that $\sum_{k=0}^{N_t} (h_k - \Delta l_k^2) / \sum_{k=0}^{N_t} l_k^2 \rightarrow 0$ as $t \rightarrow \infty$ (see Appendix A). It follows

$$\overline{\delta^2(\Delta; t)} \simeq D_t \Delta \quad (\Delta \ll t \text{ and } t \rightarrow \infty), \quad (25)$$

where $D_t = \sum_{k=0}^{N_t} l_k^2 / t$. As shown in Fig. 4, TAMSDs increase linearly with time Δ (normal diffusion), while

the diffusion coefficients show large fluctuations.

Now, we derive the PDF $P_2(z, t)$ of $Z_t \equiv \sum_{k=0}^{N_t} l_k^2$. We note that l_k^2 and N_t are mutually correlated because both of them depend on the k th trapping time, and thus we cannot apply the method used in previous studies [12, 27]. Instead, we use the fact that Z_t obeys a directed SEDLF with the joint probability

$$\psi_2(z, t) = w(t) \delta(z - t^{2\gamma}). \quad (26)$$

Therefore, in the same way as Eq. (12), we obtain

$$\hat{P}_2(k, s) = \frac{1}{s} \frac{1 - \hat{w}(s)}{1 - \hat{\psi}_2(k, s)}, \quad (27)$$

with $\hat{\psi}_2(k, s) = \int_0^\infty e^{-st} e^{ikt^{2\gamma}} w(t) dt$. Thus, the calcula-

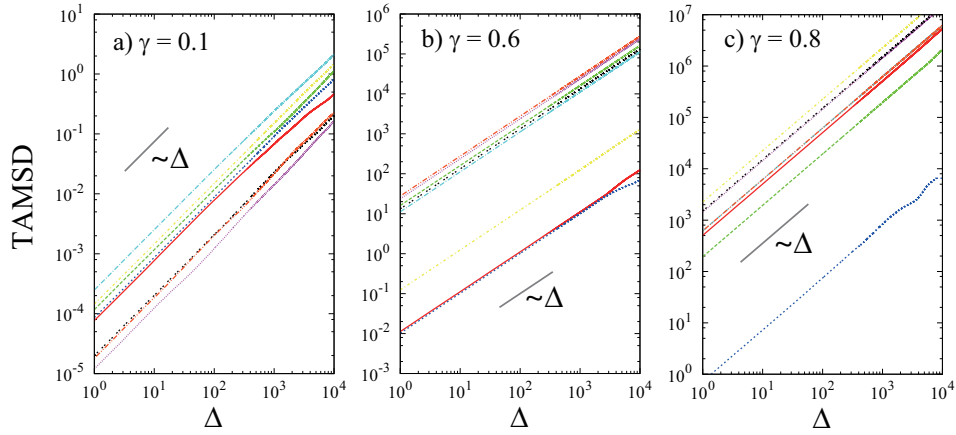


FIG. 4. Time-averaged mean square displacements ($\alpha = 0.5$ and $t = 10^6$). TAMSDs for eight different realizations are drawn in (a), (b), and (c) for $\gamma = 0.1, 0.6$ and $\gamma = 0.8$, respectively. Linear scalings are shown by the solid lines for reference. The PDF $w(t)$ used in the numerical simulation is the same as that in Fig. 2.

tions of the moments Z_t are almost parallel with the case of x_t . For example, we obtain the mean diffusion coefficient, $\langle D_t \rangle = \langle Z_t \rangle / t$, as follows:

$$\langle D_t \rangle \simeq \begin{cases} \frac{\Gamma(2\gamma - \alpha)}{|\Gamma(-\alpha)|\Gamma(1+2\gamma)} t^{2\gamma-1}, & (2\gamma > \alpha) \\ \frac{1}{|\Gamma(-\alpha)|\Gamma(1+\alpha)} t^{\alpha-1} \log t, & (2\gamma = \alpha) \\ \frac{\langle l^2 \rangle}{c\Gamma(1+\alpha)} t^{\alpha-1}, & (2\gamma < \alpha) \end{cases} \quad (28)$$

for $t \rightarrow \infty$. For $2\gamma > 1$, the diffusion coefficient enhances, otherwise it shows aging. This enhancement of diffusion coefficients is completely different from separable CTRWs [10, 11, 14, 27] and correlated CTRWs [28], both of which show only aging.

Furthermore, the second moment of D_t is given by

$$\langle D_t^2 \rangle \simeq \begin{cases} \frac{\Gamma(4\gamma - \alpha)|\Gamma(-\alpha)| + 2\Gamma(2\gamma - \alpha)^2}{\Gamma(4\gamma + 1)|\Gamma(-\alpha)|^2} t^{4\gamma-2}, & (2\gamma > \alpha) \\ \frac{2}{\Gamma(2\alpha + 1)|\Gamma(-\alpha)|} (t^\alpha \log t)^2, & (2\gamma = \alpha) \\ \frac{2\langle l^2 \rangle^2}{c^2\Gamma(2\alpha + 1)} t^{2(\alpha-1)}. & (2\gamma < \alpha) \end{cases} \quad (29)$$

It follows that the relative standard deviation (RSD) of D_t , $\sigma_{EB} \equiv \sqrt{\langle D_t^2 \rangle - \langle D_t \rangle^2} / \langle D_t \rangle$, which is an ergodicity breaking parameter [11, 12, 14, 29, 30], remains constant as $t \rightarrow \infty$:

$$\sigma_{EB} \simeq \begin{cases} \sqrt{\left[\frac{\Gamma(4\gamma - \alpha)|\Gamma(-\alpha)|}{\Gamma(2\gamma - \alpha)^2} + 2 \right] \Phi(2\gamma) - 1} & (2\gamma > \alpha) \\ \sqrt{2\Phi(\alpha) - 1} & (2\gamma \leq \alpha), \end{cases} \quad (30)$$

where $\Phi(x) \equiv \Gamma(x+1)^2 / \Gamma(2x+1)$. As shown in Fig. 5, the RSDs of D_t depend on γ , and they are different from that in CTRW when $2\gamma > \alpha$. Moreover, when $2\gamma = 1$, distributional behavior of diffusion coefficients of TAMSDs appears intrinsically whereas the EAMSD is normal.

In a way similar to the calculation for x_t , we can obtain all the higher moments of D_t . In particular, for $2\alpha < \gamma$,

$$\langle D_t^n \rangle \simeq \frac{n! \langle l^2 \rangle^n}{c^n \Gamma(n + \alpha)} t^{n(\alpha-1)}. \quad (31)$$

Therefore, the distribution of the scaled diffusion coefficient $D \equiv D_t / \langle D_t \rangle$ converges to the Mittag-Leffler distribution, i.e., the Laplace transform of the random variable D is given by

$$\langle e^{zD} \rangle = \sum_{n=0}^{\infty} \frac{\Gamma(1 + \alpha)^n z^n}{\Gamma(1 + n\alpha)}. \quad (32)$$

Moreover, for $2\gamma > \alpha$, the distribution of D also converges to a time-independent non-trivial distribution as $t \rightarrow \infty$, indicating that the scaled diffusion coefficient converges to a random variable (i.e., distributional ergodicity). PDFs of the normalized diffusion coefficient D for different parameters are shown in Fig. 6 by numerical simulations. PDFs depend crucially on the coupling parameter γ for $2\gamma > \alpha$. We note that the PDF for $2\gamma < \alpha$ is exactly the same as the Mittag-Leffler distribution of order α .

V. CONCLUSION

In conclusion, we have shown subdiffusion as well as superdiffusion in the SEDLF using Laplace analysis. By numerical simulations, we have presented the asymptotic behaviors of the PDF of the normalized positions in the SEDLF. This model (SEDLF) removes unphysical situations in Lévy flight such that the EAMSD always diverges. In the SEDLF, we have shown that TAMSDs increase linearly with time and the diffusion coefficients converge in distribution (distributional ergodicity). Distributions of the diffusion coefficients depends not only

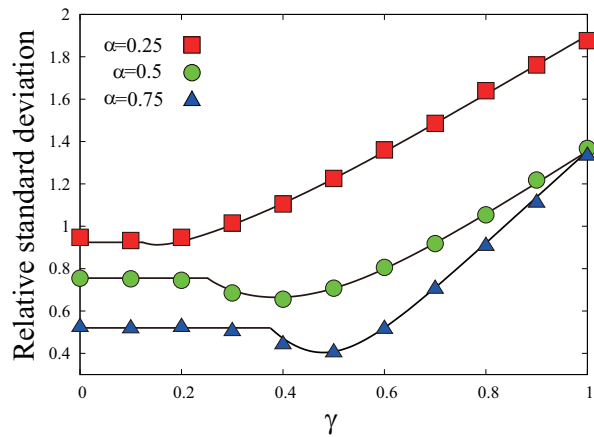


FIG. 5. Relative standard deviation of D_t as a function of γ ($\alpha = 0.25, 0.5$, and 0.75). Symbols are results of numerical simulations. We calculate D_t by $\overline{\delta^2(\Delta; t)}/\Delta$ in numerical simulations with $\Delta = 10^3$. Solid lines are theoretical curves (30). The PDF $w(t)$ used in the numerical simulation is the same as that in Fig. 2.

on the exponent α of the trapping-time distribution but also on the coupling exponent γ for $2\gamma > \alpha$, and thus are different from those in separable CTRWs [11] as well as random walks with static disorder [14]. Especially, in superdiffusive regime ($\gamma > 0.5$), the mean diffusion coefficient enhances according to the increase of the measurement time.

Appendix A: Derivation of Eq. (25)

Here, we derive Eq. (25). For $\gamma \in (0, \alpha/2)$, because of $\langle l_k^2 \rangle < \infty$, both terms

$$\frac{1}{n} \sum_{k=1}^n \Delta l_k^2 \quad \text{and} \quad \frac{2}{n} \sum_{k=1}^n \sum_{m=1}^{k-1} l_k l_m \theta(\Delta - t_k + t_m) \quad (\text{A1})$$

converge to their ensemble averages as $n \rightarrow \infty$ thanks to the law of large numbers. Moreover, the first term is dominant over the second because the ensemble average of the second term is 0 from $\langle l_k \rangle = 0$. Thus, we obtain the approximation given by Eq. (25).

For $\gamma \in (\alpha/2, \alpha)$, the first term diverges as $n \rightarrow \infty$ because of $\langle l_k^2 \rangle = \infty$, while the second term remains finite. Thus, in this case too, the first term is dominant and Eq. (25) is valid.

For $\gamma \in (\alpha, 1)$, the both terms diverge, but still the same approximation holds. From the generalized limit theorem for stable distributions [23], the first term scales as $\sim n^{2\gamma/\alpha-1}$, because a random variable $y = l_k^2$ is distributed according to PDF $f(y) \sim 1/y^{1+\alpha/2\gamma}$. On the other hand, the second term scales as $\lesssim n^{\gamma/\alpha-1}$ because

$$\sum_{k=1}^n \sum_{m=1}^{k-1} |l_k l_m \theta(\Delta - t_k + t_m)| < \Delta^2 \sum_{k=1}^n |l_k| \lesssim \Delta^2 n^{\gamma/\alpha},$$

where we used the generalized central limit theorem again for the scaling of $\sum_m |l_m|$ (Note that $|l_m|$ follows the PDF $p(l) \sim 1/|l|^{1+\alpha/\gamma}$). We also used the facts that $\tau_k + \dots + \tau_{m+1} \leq \Delta$ if $\theta(\Delta - t_k + t_m) > 0$, where $\tau_k \equiv t_k - t_{k-1}$. Thus, $\sum_{m=1}^{k-1} |l_m| \theta(\Delta - t_k + t_m) = \sum_{m=1}^{k-1} \tau_m^\gamma \theta(\Delta - t_k + t_m) < \Delta^2$. Finally, the ratio of the second term against the first goes to zero, i.e., $n^{\gamma/\alpha-1}/n^{2\gamma/\alpha-1} = n^{-\gamma/\alpha} \rightarrow 0$ as $n \rightarrow \infty$.

-
- [1] A. Caspi, R. Granek, and M. Elbaum, Phys. Rev. Lett. **85**, 5655 (2000).
 - [2] I. Golding and E. C. Cox, Phys. Rev. Lett. **96**, 098102 (2006).
 - [3] A. Granéli, C. C. Yeykal, R. B. Robertson, and E. C. Greene, Proc. Natl. Acad. Sci. USA **103**, 1221 (2006).
 - [4] A. Weigel, B. Simon, M. Tamkun, and D. Krapf, Proc. Natl. Acad. Sci. USA **108**, 6438 (2011).
 - [5] J.-H. Jeon, V. Tejedor, S. Burov, E. Barkai, C. Selhuber-Unkel, K. Berg-Sørensen, L. Oddershede, and R. Metzler, Phys. Rev. Lett. **106**, 048103 (2011).
 - [6] S. C. Weber, A. J. Spakowitz, and J. A. Theriot, Proc. Natl. Acad. Sci. USA **109**, 7338 (2012).
 - [7] I. M. Zaid, M. A. Lomholt, and R. Metzler, Biophys. J. **97**, 710 (2009).
 - [8] R. Metzler and J. Klafter, Phys. Rep. **339**, 1 (2000).
 - [9] M. J. Saxton, Biophys. J. **92**, 1178 (2007).
 - [10] A. Lubelski, I. M. Sokolov, and J. Klafter, Phys. Rev. Lett. **100**, 250602 (2008).
 - [11] Y. He, S. Burov, R. Metzler, and E. Barkai, Phys. Rev. Lett. **101**, 058101 (2008).
 - [12] T. Miyaguchi and T. Akimoto, Phys. Rev. E **83**, 062101 (2011).
 - [13] Y. Meroz, I. M. Sokolov, and J. Klafter, Phys. Rev. Lett. **110**, 090601 (2013).
 - [14] T. Miyaguchi and T. Akimoto, Phys. Rev. E **83**, 031926 (2011).
 - [15] J. Aaronson, *An Introduction to Infinite Ergodic Theory* (American Mathematical Society, Providence, 1997).
 - [16] T. Akimoto and T. Miyaguchi, Phys. Rev. E **82**, 030102(R) (2010).
 - [17] M. M. Meerschaert and E. Scalas, Physica A **370**, 114 (2006).
 - [18] A. Helmstetter and D. Sornette, Phys. Rev. E **66**, 061104 (2002).

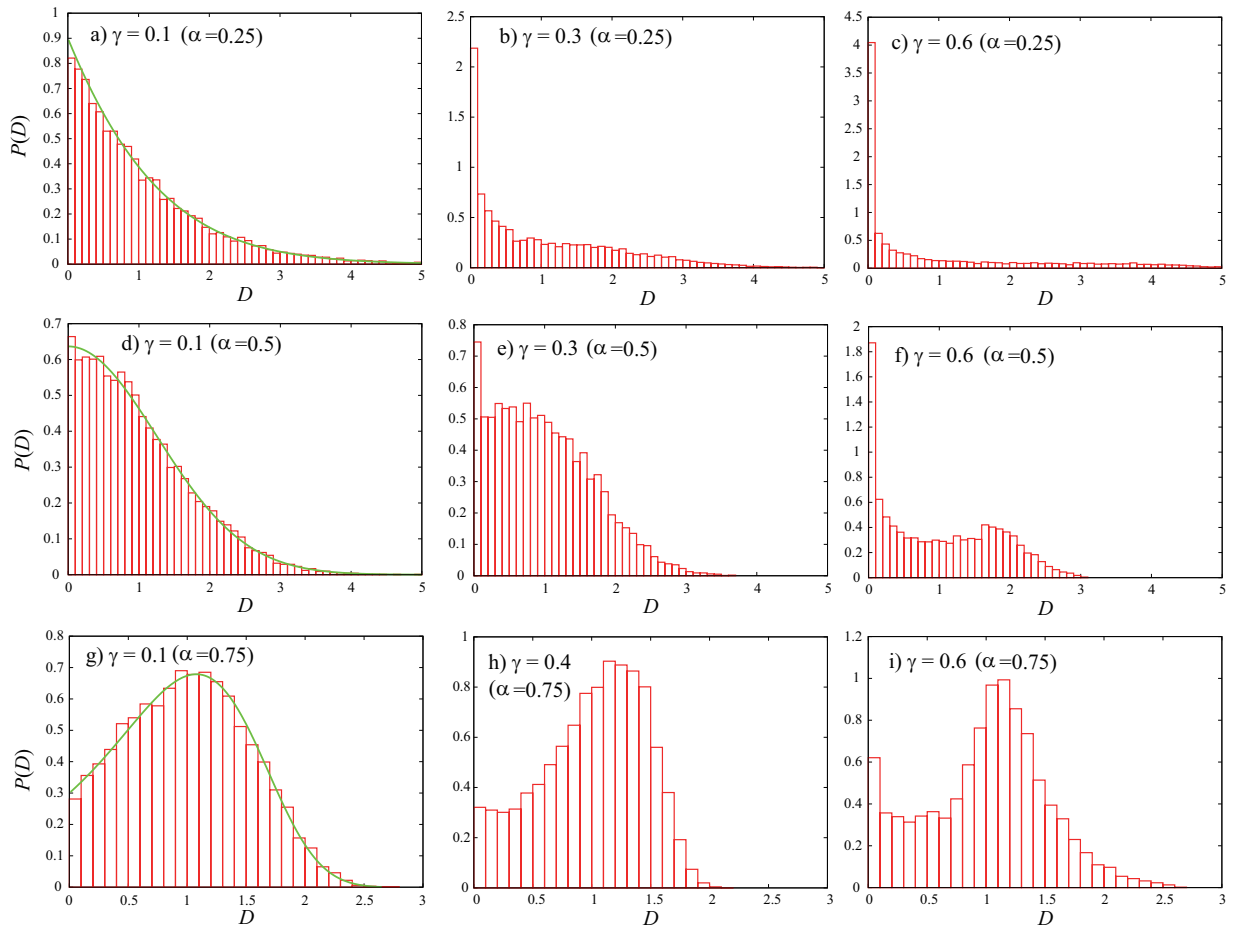


FIG. 6. Histograms of the normalized diffusion coefficients $D \equiv D_t / \langle D_t \rangle$ for different $\gamma = 0.1, 0.4, 0.6,$ and 0.8 ($\alpha = 0.25$ and 0.75). D_t is calculated in the same way as in Fig. 5. The solid curves represent the Mittag-Leffler distribution. The PDF $w(t)$ used in the numerical simulation is the same as that in Fig. 2.

- (2002).
- [19] J. Klafter, A. Blumen, and M. F. Shlesinger, Phys. Rev. A **35**, 3081 (1987).
- [20] M. Magdziarz, W. Szczotka, and P. Żebrowski, J. Stat. Phys. **147**, 74 (2012).
- [21] J. Liu and J.-D. Bao, Physica A **392**, 612 (2013).
- [22] M. Shlesinger, J. Klafter, and Y. Wong, J. Stat. Phys. **27**, 499 (1982).
- [23] J. Bouchaud and A. Georges, Phys. Rep. **195**, 127 (1990).
- [24] H. Scher and E. W. Montroll, Phys. Rev. B **12**, 2455 (1975).
- [25] D. R. Cox, *Renewal theory* (Methuen, London, 1962).
- [26] Y. Kasahara, Publ. RIMS, Kyoto Univ. **12**, 801 (1977).
- [27] T. Miyaguchi and T. Akimoto, Phys. Rev. E **87**, 032130 (2013).
- [28] V. Tejedor and R. Metzler, J. Phys. A **43**, 082002 (2010).
- [29] T. Akimoto, E. Yamamoto, K. Yasuoka, Y. Hirano, and M. Yasui, Phys. Rev. Lett. **107**, 178103 (2011).
- [30] T. Uneyama, T. Akimoto, and T. Miyaguchi, J. Chem. Phys. **137**, 114903 (2012).